Computers and Geotechnics 99 (2018) 130–136

Contents lists available at ScienceDirect

Computers and Geotechnics

journal homepage: www.elsevier.com/locate/compgeo

Technical Communication

Influence of boundary constraints on stress heterogeneity modelling

Ke Gao[a], Qinghua Lei[b,*]

[a] Department of Civil Engineering, University of Toronto, Toronto, Canada
[b] Department of Earth Science and Engineering, Imperial College London, London, United Kingdom

ARTICLE INFO

Keywords:
Boundary stiffness
Stress dispersion
Effective variance
Stress heterogeneity
Finite-discrete element method

ABSTRACT

By employing the effective variance of stress tensors as a scalar-valued measure of stress heterogeneity, we quantitatively analyse the influence of boundary constraint stiffness on numerically derived stress distribution in a fractured rock mass. The results reveal a decreasing trend in the effective variance of stress field with an increasing boundary constraint stiffness. This work demonstrates the efficacy of effective variance for stress heterogeneity quantification, and also indicates that the boundary constraint stiffness can affect stress modelling results. We suggest that quantitative evaluation of the effects of boundary constraints may be needed in geomechanical modelling of fractured rock masses.

1. Introduction

Crustal rocks, embedded with widespread natural fractures, are subjected to stresses, mainly due to the overburden and tectonic effects [1]. Thus, the *in situ* state of stress is an important parameter for a wide range of endeavours in rock mechanics [1–6]. Because of the inherent complexity of fractured rock masses in terms of varying rock properties and presence of discontinuities, the stress state often exhibits significant heterogeneity [4,7–10]. The *in situ* stress measurement results shown in Fig. 1 exemplify the dramatic variation in both the principal stress magnitude and orientation along two sides of a fault [8].

However, a thorough characterisation of stress heterogeneity in the field is very challenging, which requires sufficient and detailed *in situ* stress measurements [11]. Due to implementation difficulties and budget limits, it is often difficult to conduct a large number of stress measurements in real engineering projects. Numerical simulation provides an alternative and fast solution to this issue [11,12]. In the past few decades, many numerical models have been developed to solve different rock mechanics problems [13–15], while only a few efforts have been devoted to investigating the phenomena of stress heterogeneity [11,16–21]. In these previous geomechanical modelling studies, different types of numerical boundary constraints, e.g. stress boundary constraints [3,16,21–25], displacement boundary constraints and combined stress-displacement boundary constraints [17,18,26–28], have been assumed for simulating the geological confinement imposed by surrounding rocks onto the problem domain (e.g. Fig. 2). It is found that rare discussions were made regarding the influence of different boundary constraint types on simulation results, which needs to be examined in a quantitative manner.

In order to quantify the variability of stress tensor fields, Gao and Harrison [29,30] proposed a stress variability characterisation approach using “effective variance” as a scalar-valued measure of the overall stress heterogeneity. This metric for stress tensor data has the similar functionality to the variance and standard deviation of scalar data. This effective variance approach has proven its accuracy and robustness in quantifying stress heterogeneity in complex geological media [29–31].

In this paper, we use the two-dimensional (2D) finite-discrete element method (FEMDEM) [32,33] to simulate the stress distribution in a fractured rock mass subjected to different types of boundary constraints. We employ the effective variance method to quantify the influence of boundary constraint stiffness on the simulated stress results. We aim to draw attention from the community to the potentially important effects of boundary constraint on geomechanical modelling. In the rest of the paper, we first introduce the effective variance method in Section 2, followed by a brief description of the FEMDEM approach in Section 3. We then present the model setup and simulation results in Section 4. Finally, a few concluding remarks are presented.

2. Effective variance – scalar-valued stress dispersion quantification

As mentioned earlier, stress in rock masses often displays significant heterogeneity. It is important that such heterogeneity can be characterised in a quantitative manner [34–37]. Dispersion, which denotes how scatter or spread out a data group is with respect to its mean, is an

* Corresponding author.
E-mail address: q.lei12@imperial.ac.uk (Q. Lei).

https://doi.org/10.1016/j.compgeo.2018.03.003
Received 8 November 2017; Received in revised form 11 February 2018; Accepted 11 March 2018
Available online 16 March 2018
0266-352X/

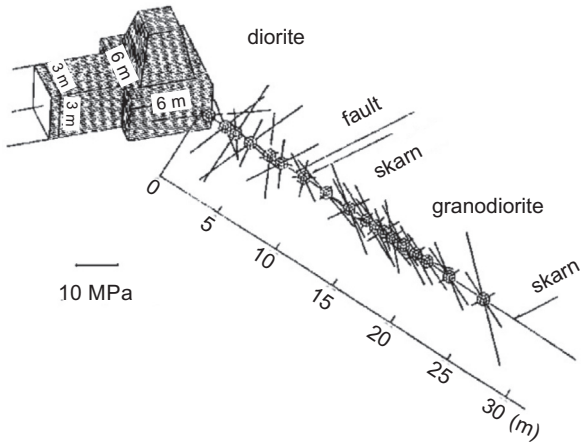

Fig. 1. Dramatic stress change observed near a fault. Note that the pairs of orthogonal intersecting lines represent the principal stress orientations and their length denote the principal stress magnitudes at different locations [8].

effective parameter for such characterisation. However, stress is tensor in nature formed by six distinct components. The conventional decoupled analysis of principal stress magnitude and orientation, which was usually adopted in the literature [38–41], may lead to biased assessment results [29,31,34,36,42,43].

To tackle this problem, considering that the variability of stress tensors can be adequately represented by the variability of its distinct tensor components in a multivariate manner [43], Gao and Harrison [29,30] proposed to employ the concept of "effective variance" for stress variability characterisation. The method of effective variance originated from the research field of multivariate statistics for group dispersion measure [44]. The effective variance of stress tensors can be calculated based on the covariance matrix of their distinct tensor components referred to a common Cartesian coordinate system. The detailed procedure is described as follows.

For a stress tensor

$$\mathbf{S} = \begin{bmatrix} \sigma_x & \tau_{xy} & \tau_{xz} \\ & \sigma_y & \tau_{yz} \\ \text{symmetric} & & \sigma_z \end{bmatrix}, \tag{1}$$

its distinct tensor components can be obtained as

$$\begin{aligned} \mathbf{s}_\mathrm{d} &= \mathrm{vech}(\mathbf{S}) = [\sigma_x \ \ \tau_{yx} \ \ \tau_{zx} \ \ \sigma_y \ \ \tau_{zy} \ \ \sigma_z]^T \\ &= [\sigma_x \ \ \tau_{xy} \ \ \tau_{xz} \ \ \sigma_y \ \ \tau_{yz} \ \ \sigma_z]^T \end{aligned}. \tag{2}$$

Here, the subscript "d" denotes "distinct", $[\cdot]^T$ represents the matrix transpose, and $\mathrm{vech}(\cdot)$ is the half-vectorisation function which stacks only the lower triangular (i.e. on and below the diagonal) columns of a tensor into column vector containing only its distinct components [45, p. 246]. For the stress vector $\mathbf{s}_\mathrm{d}$, its covariance matrix is

$$\mathbf{\Omega} = \mathrm{cov}(\mathbf{s}_\mathrm{d}) = \frac{1}{n}\sum_{i=1}^{n} (\mathbf{s}_{\mathrm{d}i} - \bar{\mathbf{s}}_\mathrm{d}) \cdot (\mathbf{s}_{\mathrm{d}i} - \bar{\mathbf{s}}_\mathrm{d})^T, \tag{3}$$

where $\bar{\mathbf{s}}_\mathrm{d}$ denotes the mean vector and can be calculated by

$$\bar{\mathbf{s}}_\mathrm{d} = \frac{1}{n}\sum_{i=1}^{n} \mathbf{s}_{\mathrm{d}i}. \tag{4}$$

Based on the covariance matrix $\mathbf{\Omega}$ given in Eq. (3), the effective variance is defined as

$$V_{\mathrm{e|d}} = \sqrt[\frac{1}{2}p(p+1)]{|\mathbf{\Omega}|}, \tag{5}$$

where $|\cdot|$ denotes the matrix determinant and p ($p = 2$ or 3) is the dimension of the stress tensor.

The effective variance has the same unit as the variance of the stress tensor components, i.e. square of the unit of stress. Similar to the variance and standard deviation of scalar data, the larger the effective variance, the more dispersed the stress tensor data would be.

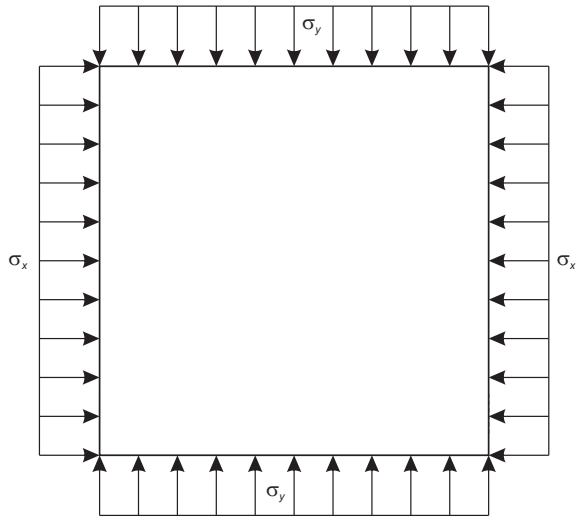

(a) Boundary loading acting directly on the rock model [3, 16, 21-25]

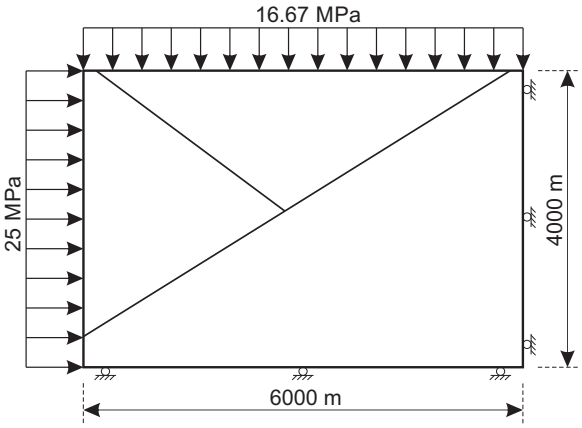

(b) Direct loading and roller boundary on the rock model [17]

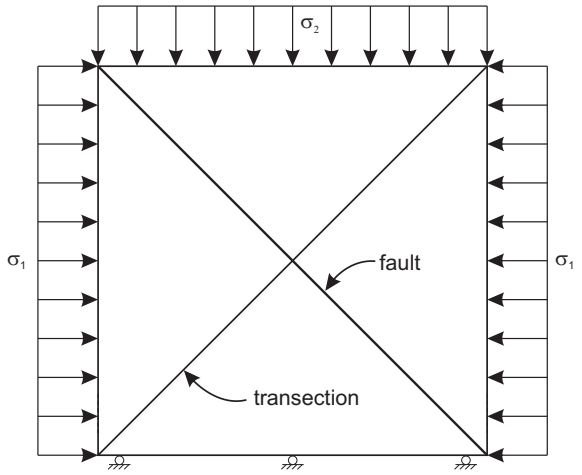

(c) Direct loading and roller boundary on the rock model [18, 26]

Fig. 2. Various boundary constraints have been used in geomechnical modelling in the literature.

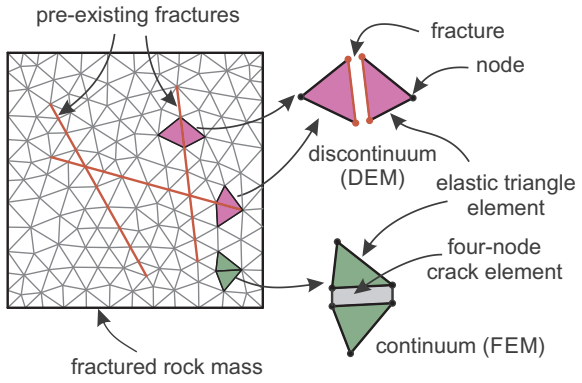

Fig. 3. Schematic illustration of the FEM and DEM modules in the FEMDEM framework.

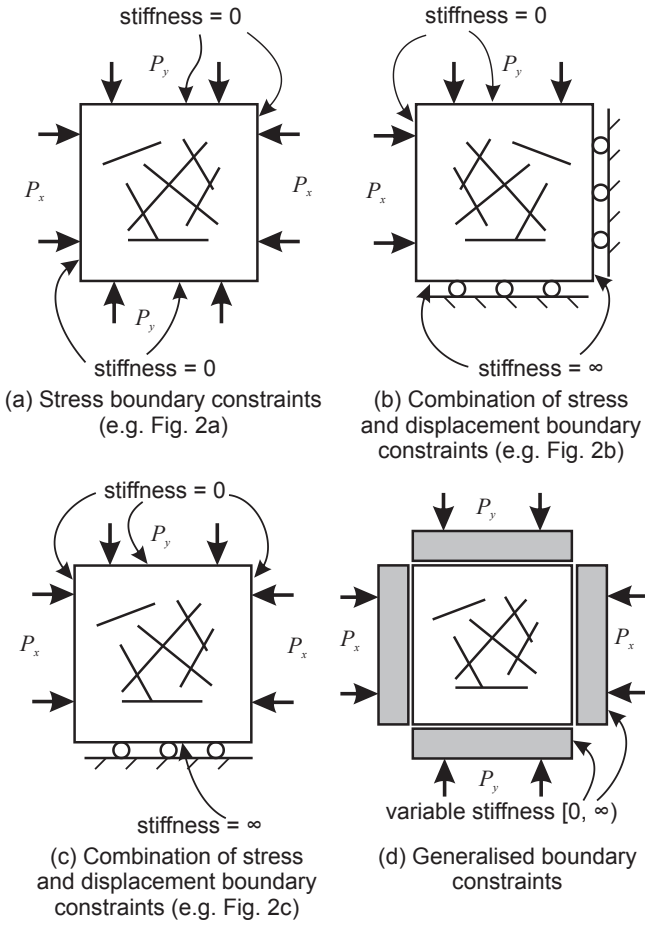

Fig. 4. Simplification of the various boundary constraint types used in existing geomechnical modelling (Fig. 2) and their generalisation from a boundary constraint stiffness point of view.

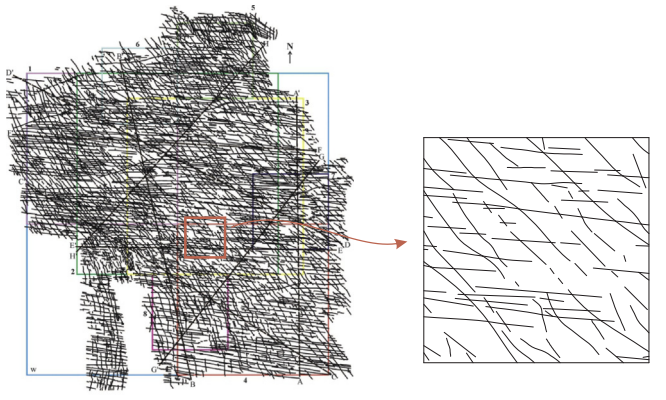

Fig. 5. The 1.5 × 1.5 m rock mass model from an outcrop in the southern margin of Bristol Channel Basin [51].

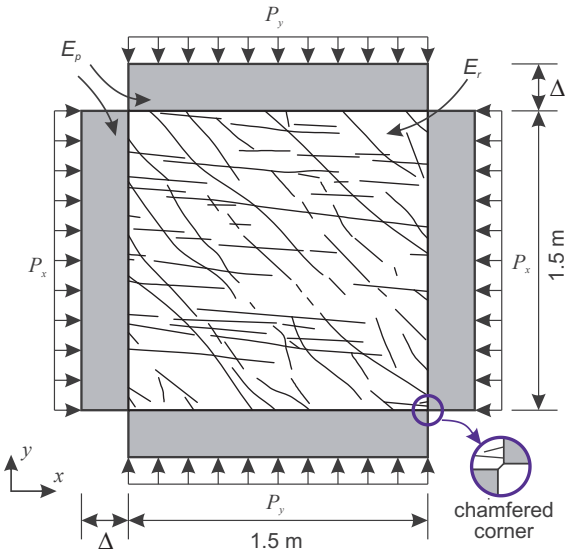

Fig. 6. Schematic description of the model used for stress simulation.

Table 1
Material properties of the rock mass.

Properties	Value	Unit
Density	2700	kg/m^3
Young's modulus E_r	30	GPa
Poisson's ratio	0.27	–
Joint friction coefficient	0.7	–
Internal friction coefficient of intact rock	0.8	–
Cohesion of intact rock	20	MPa
Tensile strength of intact rock	15	MPa
Energy release rate	800	J/m^2

3. Finite-discrete element method (FEMDEM)

The numerical model in this work is based on the finite-discrete element method (FEMDEM) originally developed by Munjiza and his colleagues [33]. The FEMDEM model represents a 2D solid using a fully discontinuous mesh of three-node triangular finite elements, which are linked by four-node crack elements (Fig. 3) [6,46]. The motions of finite elements are governed by the forces acting on elemental nodes. The governing equation is given by [33]:

$$\mathbf{M}\ddot{\mathbf{x}} + \mathbf{f}_{\text{int}} = \mathbf{f}_{\text{ext}}, \tag{6}$$

where $\mathbf{M}$ is the lumped nodal mass matrix, $\mathbf{x}$ is the vector of nodal displacements, $\mathbf{f}_{\text{int}}$ are the internal nodal forces induced by the deformation of triangular elements, $\mathbf{f}_{\text{ext}}$ are the external nodal forces including external loads $\mathbf{f}_l$ contributed by boundary conditions and body forces, cohesive bonding forces $\mathbf{f}_b$ caused by the deformation of crack elements, and contact forces $\mathbf{f}_c$ generated by the contact interaction between discrete elements.

The deformation of bulk materials is captured by elastic constant-strain triangular finite elements and solved using the finite strain formulation [33]. The contact force between two triangular elements interacting with each other is computed based on the penalty function method [33]. The Mohr-Coulomb model with tension cut-off is employed to define the shear and tensile strength of the rock [47]. The

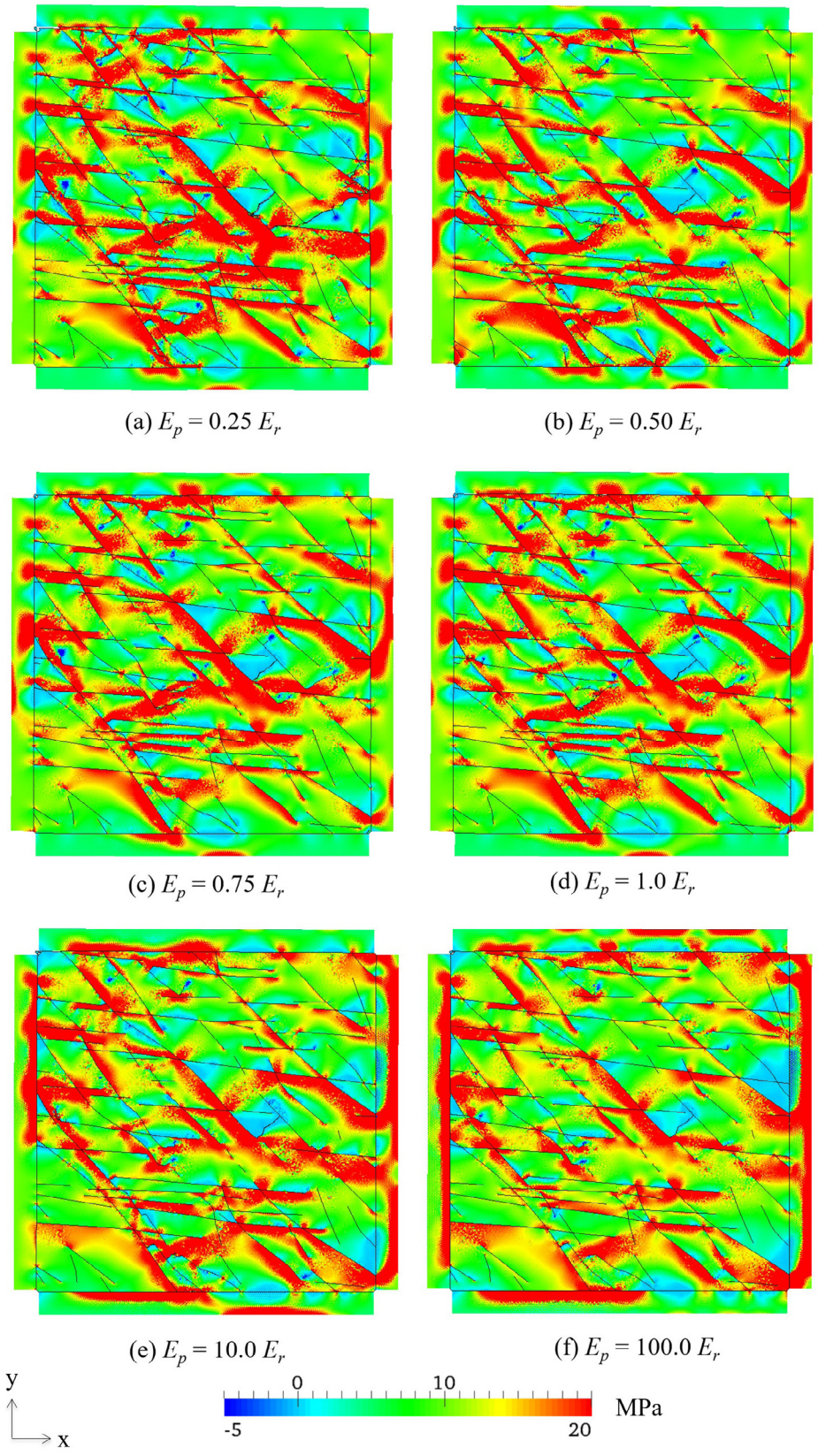

Fig. 7. Distribution of major principal stress σ_1 in the fractured rock and boundary plates associated with different constraint stiffness under loading stresses of P_x = 10 MPa and P_y = 5 MPa.

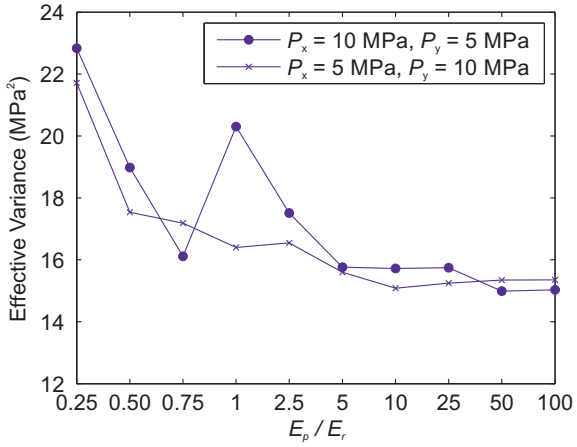

Fig. 8. Effective variance of the simulated stress data with respect to Young's modulus ratio E_p/E_r for boundary plates with a thickness of $\Delta = 0.1$ m (note that the x-axis is not designed for scale).

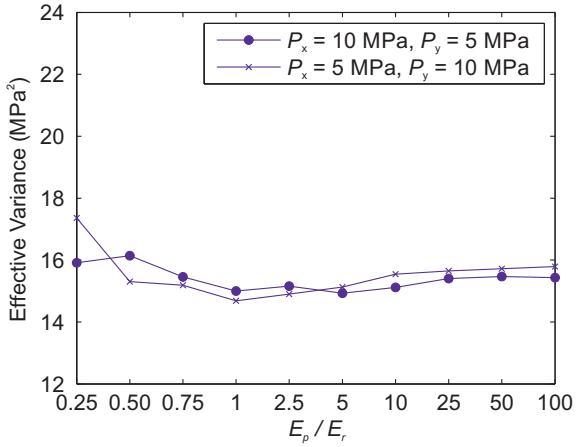

Fig. 9. Effective variance of the simulated stress data with respect to Young's modulus ratio E_p/E_r for boundary plates with a thickness of $\Delta = 0.3$ m (note that the x-axis is not designed for scale).

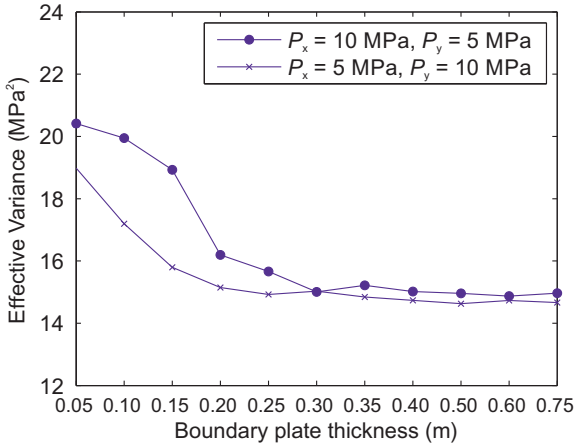

Fig. 10. Effective variance of the simulated stress data with respect to boundary plate thickness when using $E_p = E_r$.

smeared crack model embedded in the FEMDEM formulation further permits the simulator to capture the emergence of new fracturing driven by stress concentrations at fracture tips [48], which avoids the generation of unrealistic high stress concentrations at fracture tips and thus makes it an ideal tool for stress heterogeneity simulation. FEMDEM has proven its efficiency and reliability as a computational tool to solve various rock mechanics problems such as stress analysis [3,11], stress effects on rock mass permeability [3,6,21,49] and rock fracture behaviour [21,46,50].

4. Generalised boundary constraint, model setup and simulation results

4.1. Generalised boundary constraint

When building numerical models to simulate a fractured rock in a compressive state, both stress boundary constraints (i.e. stress loaded on the model boundary directly, Fig. 2a–c) [3,16,21–25] and displacement boundary constraints (i.e. roller boundary condition, Fig. 2b and c) [17,18,26–28] have been used. The first type prescribes the stress values at the model boundary whilst allowing it to displace freely; the second prohibits the model boundary from moving in a normal direction, but the stresses at the boundary are unconstrained.

All these boundary conditions may be discriminated by using the concept of boundary constraint stiffness (Fig. 4a–c). In other words, they can be generalised as boundary plates with variable stiffness that confining the fractured rock mass (Fig. 4d). This stiffness theoretically could vary from zero to infinity by changing the Young's modulus and thickness of the loading plates. Zero stiffness (i.e. zero boundary plate thickness) corresponds to the stress boundary constraint, while infinite stiffness (i.e. infinite Young's modulus or infinite thickness for boundary plates) is equivalent to the displacement boundary constraint. By adjusting the stiffness of each plate (Fig. 4d), all the different boundary conditions shown in Fig. 2 can be incorporated. In reality, the problem domain is embedded in the geological system and subjected to both stress and displacement constraints. Thus, it is useful to understand the effects of boundary constraint stiffness on the geomechanical response of fractured media.

4.2. Model setup

The fractured rock mass model used in the present investigation is generated based on an outcrop of fractured limestone on the southern margin of the Bristol Channel Basin, UK [51]. The original whole outcrop has dimensions of approximately 15 m in both *x*- and *y*-directions, and contains two conjugate fracture sets striking approximately 140° and 100°, respectively (Fig. 5a). To reduce computational cost, a 1.5 × 1.5 m domain is selected (Fig. 5b). By employing the generalised boundary constraint as shown in Fig. 4d, four identical plates with adjustable stiffness are placed on each side of the model domain and subjected to uniform compressive loadings (Fig. 6). The boundary loadings were increased gradually until they reached the target values. The boundary plates are modelled as isotropic, elastic materials, and their stress and deformation are calculated based on the finite strain formulation [33]. The interaction between the boundary plate and the rock specimen is computed using the penalty function method [33], such that the normal loading are transmitted from the boundary plate to the rock via their interface. The friction coefficient at the plate-rock interface is set zero, so no frictional force is generated at the rock periphery. To avoid contact of adjacent plates during the loading process, small chamfered corners with an edge length of 1 cm (0.67% of the rock mass edge length) are cut at the four corners of the rock model. This size of chamfered corner was carefully chosen after several trials to make it small enough to minimise the influence on stress results and large enough to avoid plate contact after deformation.

The rock mass is discretised using an unstructured triangular mesh (72,272 elements in total) with an average element edge length of ~1 cm. Material properties of the rock mass are presented in Table 1. For simplicity, the four boundary plates are chosen to have identical constraint stiffness in each simulation, which is defined by the Young's modulus E_p and thickness Δ of the plates. The larger the Young's

modulus E_p and plate thickness Δ, the stiffer is the boundary constraint. We speculate that for stiffer boundary constraint, the rock mass tends to be tighter and the perturbation of discontinuities to stress becomes less significant, with the result that the stress will be relatively more homogeneous with a smaller dispersion.

When the model reaches equilibrium, the stress tensor of each constant-strain element in the rock mass domain is extracted and their effective variance calculated. The idealised stress boundary constraint (i.e. zero boundary constraint stiffness corresponding to $E_p = 0$ and $\Delta = 0$, Fig. 2a) and displacement boundary constraint (i.e. infinite boundary constraint stiffness corresponding to $E_p = \infty$ and/or $\Delta = \infty$, Fig. 2b and c) are not examined here.

4.3. Simulation results

To explore the influence of boundary constraint stiffness on stress dispersion in the fractured rock mass, we first choose a relatively small thickness for the boundary plates, say $\Delta = 0.1$ m, and vary the Young's modulus ratio between the plates and rock (i.e. E_p/E_r) from 0.25 to 100. Fig. 7 shows some typical results of the distribution of major principal stress σ_1 in the fractured rock and boundary plates under loading stresses of $P_x = 10$ MPa and $P_y = 5$ MPa. It can be seen that with the increase of boundary stiffness, the stress distribution in the rock becomes less dispersed because of the enhanced restriction from the boundary plates against the sliding of fractures. Furthermore, the high stress zones in the plates seem to emerge close to the ends of those fractures that intersect with the plate-rock interface, and the stress concentration in the plates becomes stronger as the boundary stiffness increases.

We then calculate the effective variance of the stress fields. The variation of effective variance with respect to the plate/rock Young's modulus ratio for $P_x = 10$ MPa and $P_y = 5$ MPa, and $P_x = 5$ MPa and $P_y = 10$ MPa using boundary plate thickness of 0.1 m are presented in Fig. 8. It is found that the Young's modulus of the boundary plates has a significant influence on stress dispersion. Generally, as the plate Young's modulus increases, the effective variance decreases. This agrees with our speculation earlier – the larger the boundary constraint stiffness, the smaller is the effective variance. The effective variance asymptotically approaches to a plateau with further increase of the plate modulus (Fig. 8). The oscillatory variation of the effective variance between $E_p/E_r = 0.75$ and 2.5 for $P_x = 10$ MPa and $P_y = 5$ MPa may be related to the instability caused by the reactivation of the two pre-existing fracture sets at around $E_p/E_r = 1$.

Then, thicker boundary plates with thickness of $\Delta = 0.3$ m are used. The stress dispersion calculation results are presented in Fig. 9, which also agree with the previous speculation that in general the effective variance is decreasing with respect to the increasing Young's modulus ratio, although the change here (from 17.4 MPa^2 to 14.7 MPa^2) is not as dramatic as the ones shown in Fig. 8 (from 23.0 MPa^2 to 15.0 MPa^2). This small change of effective variance demonstrates that for thicker boundary plates, the contribution of same amount of Young's modulus change to the overall boundary constraint stiffness change is less significant.

Next, boundary plates with a Young's modulus equal to that of the rock are used to further investigate the influence of boundary plate thickness on stress dispersion as presented in Fig. 10. It shows a decreasing trend in the effective variance with the increase of the boundary plate thickness, which again demonstrates that when the boundary constraint stiffness increases, the stress dispersion decreases. In addition, when the boundary plate thickness is greater than 0.3 m, the effective variance reaches a plateau for both $P_x = 10$ MPa, $P_y = 5$ MPa and $P_x = 5$ MPa, $P_y = 10$ MPa boundary loading scenarios (Fig. 10). This is similar to the previous example for the increasing Young's modulus of boundary plates, i.e. when the boundary plate thickness continues to increase beyond a certain value, it becomes more like a rigid body; with the result that the tightness of the rock mass will not be changed notably and thus a constant stress dispersion is reached.

Overall, the simulation results clearly demonstrate that boundary constraint stiffness can significantly influence the modelling results of stress heterogeneity in a fractured rock mass. Under more compliant boundary constraints, the stress field inside the rock mass is more dispersed than that under stiffer boundary constraints.

5. Concluding remarks

We have quantitatively investigated the influence of boundary constraint stiffness on stress dispersion in a fractured rock mass using the two-dimensional FEMDEM and the effective variance as a scalar-valued measure of the degree of stress heterogeneity. We generalised the commonly used boundary constraints to a form involving four plates loading on each side of a squared rock mass model. By adjusting the loading plate stiffness, i.e. changing the thickness or Young's modulus of the plates, a series of simulations were conducted. Once the model reached equilibrium under imposed compressive boundary loadings, the complete stress tensor field of the entire domain were extracted and the effective variance calculated. The simulation results showed that the effective variance of the stress field decreases with the increasing Young's modulus and thickness of the boundary plates, implying that the stiffer the boundary constraint is, the tighter the rock mass is and thus the less dispersed the stress would be. Our observation suggests that attentions may be needed on quantifying the role of boundary constraint conditions in numerical modelling of stress distribution as well as other stress-dependent processes in fractured rock masses.

Acknowledgements

We acknowledge Prof. John P. Harrison from the University of Toronto and Dr. John-Paul Latham from the Imperial College London for the discussions and their constructive suggestions. We also thank the anonymous reviewer and the Editor D.V. Griffiths for their insightful comments that improved the manuscript.

References

[1] Amadei B, Stephansson O. Rock stress and its measurement. London: Springer; 1997.
[2] Zoback MD. Reservoir geomechanics. Cambridge: Cambridge University Press; 2010.
[3] Latham J-P, Xiang J, Belayneh M, Nick HM, Tsang C-F, Blunt MJ. Modelling stress-dependent permeability in fractured rock including effects of propagating and bending fractures. Int J Rock Mech Min Sci 2013;57:100–12.
[4] Matsumoto S, Katao H, Iio Y. Determining changes in the state of stress associated with an earthquake via combined focal mechanism and moment tensor analysis: application to the 2013 Awaji Island earthquake, Japan. Tectonophysics 2015;649:58–67.
[5] Zang A, Stephansson O. Stress field of the Earth's crust. Berlin: Springer; 2010.
[6] Lei Q, Latham J-P, Tsang C-F. The use of discrete fracture networks for modelling coupled geomechanical and hydrological behaviour of fractured rocks. Comput Geotech 2017;85:151–76.
[7] Martin CD. Characterizing in situ stress domains at the AECL Underground Research Laboratory. Can Geotech J 1990;27:631–46.
[8] Obara Y, Sugawara K. Updating the use of the CCBO cell in Japan: overcoring case studies. Int J Rock Mech Min Sci 2003;40:1189–203.
[9] Day-Lewis AD. Characterization and modeling of in situ stress heterogeneity [Ph.D. Thesis]. California, USA: Stanford University; 2008.
[10] Hyett AJ. Numerical and experimental modelling of the potential state of stress in a naturally fractured rock mass [Ph.D. Thesis]. London, UK: University of London; 1990.
[11] Harrison JP, Xiang J, Latham JP. Stress heterogeneity in a fractured rock mass modelled with the combined finite-discrete element method. 44th US rock mech symp & 5th US-Canada rock mech symp. Salt Lake City, USA: Amer Rock Mech Asso; 2010.
[12] Hart R. Enhancing rock stress understanding through numerical analysis. Int J Rock Mech Min Sci 2003;40:1089–97.
[13] Jing L. A review of techniques, advances and outstanding issues in numerical modelling for rock mechanics and rock engineering. Int J Rock Mech Min Sci 2003;40:283–353.
[14] Jing L, Hudson JA. Numerical methods in rock mechanics. Int J Rock Mech Min Sci 2002;39:409–27.

[15] Bobet A, Fakhimi A, Johnson S, Morris J, Tonon F, Yeung MR. Numerical models in discontinuous media: review of advances for rock mechanics applications. J Geotech Geoenviron 2009;135:1547–61.
[16] Hudson JA, Feng X-T. Variability of in situ rock stress. In: Xie F, editor. Rock stress and earthquakes – proc 5th int symp on in-situ rock stress. Beijing, China: CRC Press; 2010. p. 3–10.
[17] Stephansson O, Ljunggren C, Jing L. Stress measurements and tectonic implications for Fennoscandia. Tectonophysics 1991;189:317–22.
[18] Su S, Stephansson O. Effect of a fault on in situ stresses studied by the distinct element method. Int J Rock Mech Min Sci 1999;36:1051–6.
[19] Su S. Effect of fractures on in situ rock stresses studied by the distinct element method. Int J Rock Mech Min Sci 2004;41:159–64.
[20] Figueiredo B, Cornet FH, Lamas L, Muralha J. Determination of the stress field in a mountainous granite rock mass. Int J Rock Mech Min Sci 2014;72:37–48.
[21] Lei Q, Latham J-P, Xiang J, Tsang C-F, Lang P, Guo L. Effects of geomechanical changes on the validity of a discrete fracture network representation of a realistic two-dimensional fractured rock. Int J Rock Mech Min Sci 2014;70:507–23.
[22] Karatela E, Taheri A, Xu C, Stevenson G. Study on effect of in-situ stress ratio and discontinuities orientation on borehole stability in heavily fractured rocks using discrete element method. J Petrol Sci Eng 2016;139:94–103.
[23] Wu Z, Wong LNY. Frictional crack initiation and propagation analysis using the numerical manifold method. Comput Geotech 2012;39:38–53.
[24] Zhao Z, Jing L, Neretnieks I, Moreno L. Numerical modeling of stress effects on solute transport in fractured rocks. Comput Geotech 2011;38:113–26.
[25] He P, Li S-C, Li L-P, Zhang Q-Q, Xu F, Chen Y-J. Discontinuous deformation analysis of super section tunnel surrounding rock stability based on joint distribution simulation. Comput Geotech 2017;91:218–29.
[26] Lei Q, Latham J-P, Xiang J, Tsang C-F. Role of natural fractures in damage evolution around tunnel excavation in fractured rocks. Eng Geol 2017.
[27] Wu Q, Kulatilake PHSW. Application of equivalent continuum and discontinuum stress analyses in three-dimensions to investigate stability of a rock tunnel in a dam site in China. Comput Geotech 2012;46:48–68.
[28] Yao C, Shao JF, Jiang QH, Zhou CB. Numerical study of excavation induced fractures using an extended rigid block spring method. Comput Geotech 2017;85:368–83.
[29] Gao K. Contributions to tensor-based stress variability characterisation in rock mechanics [Ph.D thesis]. Canada: University of Toronto; 2017.
[30] Gao K, Harrison JP. Characterising stress dispersion for stress variability analysis. In: Johansson E, editor. RS2016 symp - 7th int symp on in-situ rock stress. Tampere, Finland: Int Soc Rock Mech; 2016.
[31] Gao K, Harrison JP. Generation of random stress tensors. Int J Rock Mech Min Sci 2017;94:18–26.
[32] Xiang J, Munjiza A, Latham J-P, Guises R. On the validation of DEM and FEM/DEM models in 2D and 3D. Eng Comput 2009;26:673–87.
[33] Munjiza AA. The combined finite-discrete element method. London: John Wiley & Sons; 2004.
[34] Gao K, Harrison JP. An aleatory model for in situ stress variability: application to two dimensional stress. In: Labuz JF, editor. 48th US rock mech/geomech symp. Minneapolis, USA: Amer Rock Mech Asso; 2014.
[35] Gao K, Harrison JP. Variability of in situ stress: the effect of correlation between stress tensor components. In: Hassani F, editor. 13th ISRM int cong rock mech. Montreal, Canada: Int Soc Rock Mech; 2015.
[36] Gao K, Harrison JP. Mean and dispersion of stress tensors using Euclidean and Riemannian approaches. Int J Rock Mech Min Sci 2016;85:165–73.
[37] Gao K, Harrison JP. Tensor variate normal distribution for stress variability analysis. In: Ulusay R, editor. ISRM int symp EUROCK 2016. Cappadocia, Turkey: Int Soc Rock Mech; 2016.
[38] Brown ET, Hoek E. Trends in relationships between measured in-situ stresses and depth. Int J Rock Mech Min Sci Geomech Abs 1978;15:211–5.
[39] Lisle RJ. The statistical analysis of orthogonal orientation data. J Geol 1989;97:360–4.
[40] Revets SA. Stress orientation confidence intervals from focal mechanism inversion. Available from: 1008.0471 2010.
[41] Zhao XG, Wang J, Cai M, Ma LK, Zong ZH, Wang XY, et al. In-situ stress measurements and regional stress field assessment of the Beishan area, China. Eng Geol 2013;163:26–40.
[42] Hyett AJ, Dyke CG, Hudson JA. A critical examination of basic concepts associated with the existence and measurement of in situ stress. In: Stephansson O, editor. ISRM int symp on rock stress & rock stress measurements. Stockholm, Sweden: Int Soc Rock Mech; 1986. p. 387–96.
[43] Gao K, Harrison JP. Multivariate distribution model for stress variability characterisation. Int J Rock Mech Min Sci 2018;102:144–54.
[44] Peña D, Rodríguez J. Descriptive measures of multivariate scatter and linear dependence. J Multivariate Anal 2003;85:361–74.
[45] Seber GA. A matrix handbook for statisticians. New York: John Wiley & Sons; 2007.
[46] Lei Q, Latham J-P, Xiang J. Implementation of an empirical joint constitutive model into finite-discrete element analysis of the geomechanical behaviour of fractured rocks. Rock Mech Rock Eng 2016;49:4799–816.
[47] Guo L. Development of a three-dimensional fracture model for the combined finite-discrete element method [Ph.D. thesis]. London, UK: Imperial College London; 2014.
[48] Munjiza A, Andrews KRF, White JK. Combined single and smeared crack model in combined finite-discrete element analysis. Int J Numer Meth Eng 1999;44:41–57.
[49] Lei Q, Latham J-P, Tsang C-F, Xiang J, Lang P. A new approach to upscaling fracture network models while preserving geostatistical and geomechanical characteristics. J Geophys Res 2015;120:4784–807.
[50] Rougier E, Knight EE, Sussman AJ, Swift RP, Bradley CR, Munjiza A, et al. The combined finite-discrete element method applied to the study of rock fracturing behavior. 3D. 45th U.S. rock mech/geomech symp. San Francisco, USA: Amer Rock Mech Asso; 2011.
[51] Belayneh MW, Matthai SK, Blunt MJ, Rogers SF. Comparison of deterministic with stochastic fracture models in water-flooding numerical simulations. AAPG Bull 2009;93:1633–48.